ACS APPLIED MATERIALS & INTERFACES

Research Article

www.acsami.org

Functionalization of SnO_2 Photoanode through Mg-Doping and TiO_2-Coating to Synergically Boost Dye-Sensitized Solar Cell Performance

Hongchang Pang,[†] HongBin Yang,[†] Chun Xian Guo,[‡,§] and Chang Ming Li*[,†,‡,§]

[†]School of Chemical and Biomedical Engineering, Nanyang Technological University, 70 Nanyang Drive, Singapore 637457.

[‡]Institute for Clean Energy & Advanced Materials, Southwest University, Chongqing 400715, China

[§]Chongqing Key Laboratory for Advanced Materials and Technologies of Clean Energies, Chongqing 400715, China

Supporting Information

ABSTRACT: Mg-doped SnO_2 with an ultrathin TiO_2 coating layer was successfully synthesized through a facile nanoengineering art. Mg-doping and TiO_2-coating constructed functionally multi-interfaced SnO_2 photoanode for blocking charge recombination and enhancing charge transfer in dye-sensitized solar cells (DSC). The designed nanostructure might play a synergistic effect on the reducing recombination and prolonging the lifetime in DSC device. Consequently, a maximum power conversion efficiency of 4.15% was obtained for solar cells fabricated with the SnO_2-based photoelectrode, exhibiting beyond 5-fold improvement in comparison with pure SnO_2 nanomterials photoelectrode DSC (0.85%).

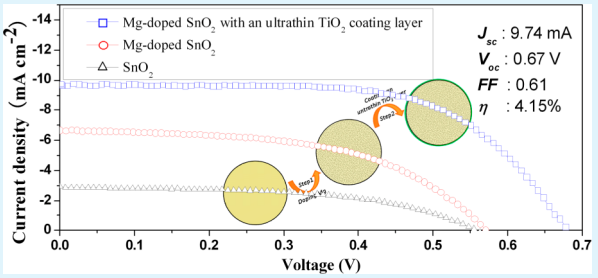

KEYWORDS: *dye-Sensitized Solar Cells, nanoengineering art, charge transfer, Mg-doping, TiO_2-coating, charge recombination*

1. INTRODUCTION

SnO_2-based nanomaterials as a promising alternative photoanode candidate for TiO_2 in dye-sensitized solar cells (DSCs) have attracted increasing attentions due to their high electron mobility (100−200 $cm^2\ V^{-1}\ S^{-1}$, 100 times higher than that of TiO_2) and large band gap (3.6 eV).[1−7] However, a DSC device with plain SnO_2 as the photoanode suffers from quite low photoelectricity conversion efficiency (less than 1%) because of faster electron recombination and significantly worse dye adsorption, leading to lower open-circuit voltage and smaller short-circuit photocurrent in comparison to TiO_2 ones.[8−13] Most recently, some unique SnO_2 nanomaterials such as nanocrystals prepared by microwave-assist approach, aligned SnO_2 nanofibers via multinozzle electrospinning method and hierarchical SnO_2 octahedral through a sonochemical process have been reported to increase the loading amount of dye molecules for a higher power conversion efficiency (PCE).[11,14,15] The PCE of SnO_2-based DSCs could also be improved by Zn-doping in SnO_2 nanocrystals to tune the sub-band gap states.[16] Moreover, coating a ultrathin insulation layer (MgO, Al_2O_3, ZrO_2, etc.) on SnO_2 nanoparticles is able to increase the sensitized photocurrent through inhibition of electron back transfer from SnO_2 to the redox electrolyte through the blocking layer.[17] Herein we present a facile method to nanoengineering functionally multi-interfaced SnO_2 photoanode through doping magnesium (Mg-SnO_2) to substantially enhance the light path for less charge recombination and subsequently coating a uniform ultrathin TiO_2 layer on the Mg-doped SnO_2 (Mg−SnO_2−TiO_2) to synergically improve DSC performance. Through material characterization and electrochemical analysis, the synergic enhancement mechanism is proposed. The DSC device using Mg-SnO_2−TiO_2 photoanode achieves an overall PCE of 4.15%, which is remarkably a 5-fold improvement over the SnO_2-based ones.

2. EXPERIMENTAL SECTION

Materials. Tin(IV) oxide and magnesium oxide were purchased from Sigma-Aldrich. Titanium(IV) *i*-propoxide (TTIP, 98%) was purchased from Sterm Chemicals. Absolute ethanol (AR, Fisher Scientific), 2-propanol (AR, Fisher Scientific), ammonia solution (25 wt %, Fisher Scientific), and Milli-Q water (18.2 MΩ cm) were used for the synthesis.

2.1. Preparation of Mg-Doped SnO_2 with an Ultrathin TiO_2 Coating layer. The SnO_2-based nanomaterial was prepared by two-pot hydrothermal method.[18] In a classic synthesis, SnO_2 and MgO (Mg molar ratio is 3%) were mixed into 60 mL of DI water under magnetic stirring for 5 h. And then the mixture was transferred into 100 mL capacity Teflon-lined stainless steel autoclave, sealed and heated at 180 °C for 48 h. The precipitated powders were filtered, washed, and transferred to titanium isopropoxide/ethylene glycol mixture in acetonitrile solution, and then sealed in a 100 mL stainless steel autoclave and finally heated at 150 °C for 20 h. The precipitate was centrifugalized and dried. And then the powder was calcined at 750 °C for 2 h.

2.2. Preparation of Photoanode and Cell Assembly. All pastes of pure SnO_2, Mg-doped SnO_2, and Mg-doped SnO_2 with an ultrathin

Received: September 1, 2012
Accepted: October 16, 2012
Published: October 16, 2012

   dx.doi.org/10.1021/am3018493 | ACS Appl. Mater. Interfaces 2012, 4, 6261−6265

TiO_2 coating layer were conducted according to the previous literature.[8] The thin films were uniformly spread on the surface of the precleaned FTO glass by the doctor-blade technique, subsequently sintered at 450 °C in air for 30 min. Subsequently, the prepared photoelectrodes were soaked in an acetonitrile solution containing 0.5 mM N719 dye at room temperature for 24 h, and then washed with ethanol and dried in dry air. Finally, the DSCs were assembled from SnO_2-based photoelectrode to Pt counter electrode with a spacer of 30 μm thickness with 5 μL of the I^-/I_3^- electrolyte solution for further characterization.

2.3. Characterization of Samples. The morphology of the samples was tested by field-emission scanning electron microscope (FE-SEM, JSM-6700F) and transmission electron microscope (TEM, Tecnai G^2 20 instrument). The XRD pattern was conducted using Rigaku D/max 2400 X-ray diffractometer equipped with graphite monochromatized Cu Kα radiation (λ = 1.5406 Å). A scan rate of 0.02° s^{-1} was applied to record the pattern in the 2θ range from 10° to 80°. The characteristics of current density (J) versus voltage (V) were measured by Keithley 2420 in dark and under illumination of an Oriel solar simulator with 100 mW cm^{-2} AM1.5G spectrum as well. The intensity of the solar simulator was calibrated by standard Si photovoltaic cell. The area of all tested devices was 16 mm^2. All measurements were carried out in air at room temperature without encapsulation.

3. RESULTS AND DISCUSSION

As well-known, pure SnO_2 as the photoanode commonly exhibits lower open-circuit voltage and smaller short-circuit photocurrent owing to faster electron recombination and significantly worse dye adsorption. Hence, great efforts are concurrently required to explore SnO_2-based materials for high power conversion efficiency in DSC devices. Our strategy for improving the PCE of SnO_2 photoanode can be realized by nanoengineering functionally multi-interfaced SnO_2, which involves two main procedures (illustrated in Figure 1). First,

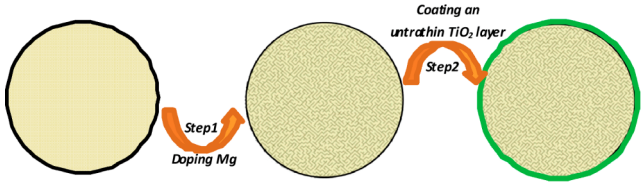

Figure 1. Schematic of the fabrication procedure of nanoengineering functionally multi-interfaced Mg-doped SnO_2 with an ultrathin TiO_2 coating layer.

magnesium doping could divide SnO_2 nanocrystals into subunits by a direct hydrothermal process of SnO_2 and MgO. The effect of doping magnesium is more like to prolong the path of electron transfer in SnO_2 nanocrystals, leading to less recombination. Subsequently, coating an ultrathin TiO_2 layer on the Mg-doped SnO_2 nanoparticle through in situ hydrolysis might improve dye adsorption and further block electron recombination, synergistically enhancing the performance of DSC device.

The X-ray diffraction (XRD) pattern (Figure 2) of the Mg-doped SnO_2 nanomaterial shows that most of the brag peaks are consistent with those of the tetragonal SnO_2 phase (space group $P4_2/mnm$, a = 4.7382 Å, c = 3.1871 Å, JCPDS No. 41−1445). After coating the ultrathin TiO_2 layer, some minor peaks corresponding to the anatase (JCPDS No. 21−1272) can also be observed in the XRD pattern, whereas no dopant peaks such as magnesium oxide and magnesium stannate were detected.

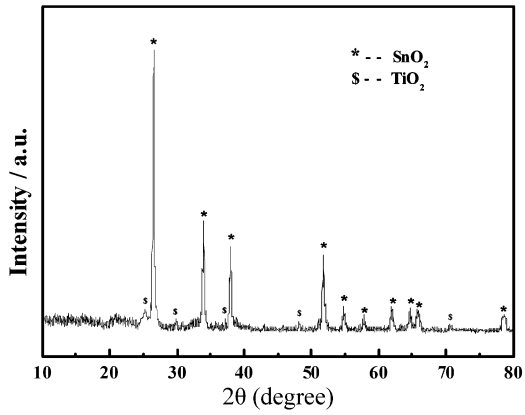

Figure 2. XRD pattern of Mg-doped SnO_2 with an ultrathin TiO_2 coating layer.

This is very likely to attribute to the inconspicuous lattice distortion.

The scanning electron microscopy (SEM) image of the Mg−SnO_2−TiO_2 power, a Mg-doped powder with the ultrathin TiO_2 coating (Figure 3a) indicates that the nanocomposite can

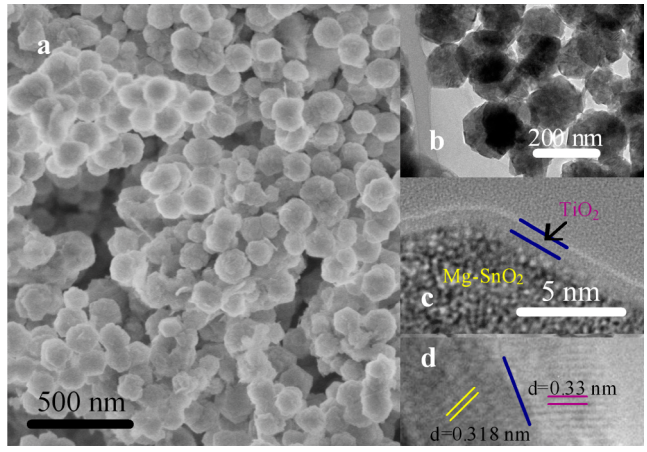

Figure 3. (a) SEM, (b, c) TEM images, and (d) HRTEM of Mg-doped SnO_2 with an ultrathin TiO_2 coating layer.

be fabricated at a large scale with an average diameter of 100 nm. No significantly morphological difference from the Mg-SnO_2 nanoparticles is observed. The microstructure and composition of the Mg-SnO_2−TiO_2 nanocomposite were further studied by TEM and HRTEM. The low magnification TEM image in Figure 3b shows uniform torispherical nanoparticles. The amplified TEM image (Figure 3c) specifies a 1−2 nm homogeneous ultrathin coating layer on the Mg-doped SnO_2 nanoparticle. To confirm the distribution of SnO_2 and TiO_2, HRTEM characterization was carried out at different locations. As shown in Figure 3d, these two HRTEM images reveal (110) lattice planes of SnO_2 and (110) lattice planes of TiO_2, respectively.

The X-ray photoelectron spectroscopy (XPS) (Figure 4) revealed the intrinsic characteristic of Mg doping SnO_2 with an ultrathin TiO_2 layer. It is clearly shown that remarkable peaks correspond to tin, magnesium, titanium and oxygen. The peaks at 485.03 and 493.46 eV exactly correspond to the binding energies of Sn $3d_{5/2}$ and Sn $3d_{3/2}$, respectively. The twin peaks exhibited spin orbit coupling. And the binding energy shift

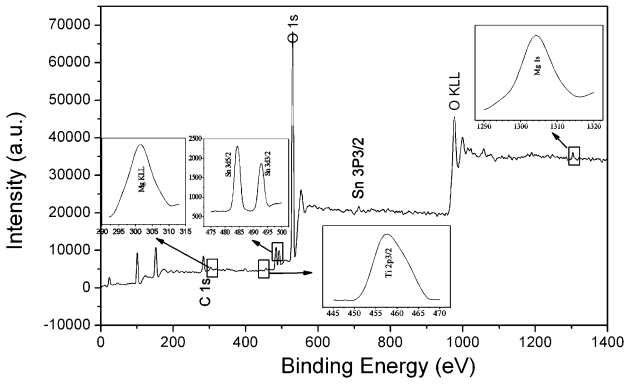

Figure 4. XPS spectra of Mg-doped SnO_2 with an ultrathin TiO_2 coating layer photoelectrodes. The insets from left to right showing Mg KLL, doubly split Sn 3d orbit, Ti 2p orbit, and Mg 1s orbit, respectively.

distincted from the standard reference value could be attributed to the variety of crystal field around Sn atoms.[19] More importantly, Mg 1s peak and Mg KLL peak are arose at 1303.68 and 303.43 eV, respectively, strongly verifying the Mg atoms doping into SnO_2 crystal lattice by replacing Sn positions.[20,21] In addition, the peak corresponding to binding energy of Ti $2p_{3/2}$ appears at 458.57 eV, which indicates intimate combination between SnO_2 core and TiO_2 coating layer. Thus, on the basis of the XPS spectra, it can be confirmed that Mg-doping state in SnO_2 nanocrystals and TiO_2 closely coating on the surface of SnO_2.

To demonstrate the photovoltaic performance, we doctor blade-printed various tailored SnO_2-based nanomaterials on FTO substrates as the DSC photoanodes and were evaluated under an illumination of one sun condition (AM 1.5 globe, 100 mW cm^{-2}). The structure of device is illustrated in the Figure 5a. The enlarged SEM image of cross-section (Figure 5b) shows a relatively uniform distribution of pores among the nanoparticles. The situation of filled holes by electrolyte could be observed in the Figure 5c. Furthermore, energy-dispersive X-ray spectroscopy (EDX) shown in Figure 5d also verified the

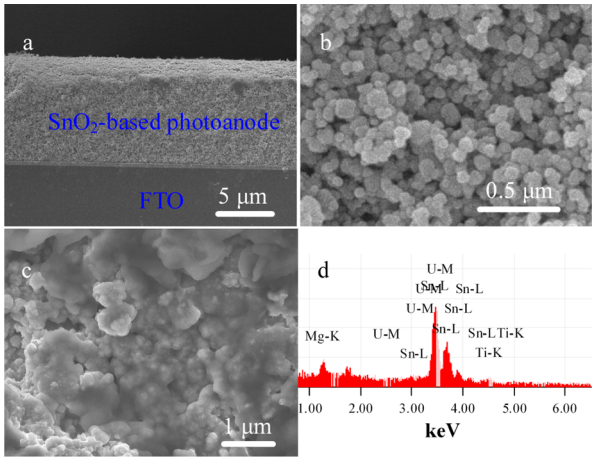

Figure 5. SEM images (a, b) of cross-section of DSCs based on the Mg-doped SnO_2 with an ultrathin TiO_2 coating layer photoelectrodes. (c) SEM image of cross-section of SnO_2-based photoelectrode with absored N719 dye. (d) Energy-dispersive X-ray spectroscopy (EDX) corresponding to the nanoengineering functionally SnO_2 nanoparticles.

component of nanoengineering functionally SnO_2 nanoparticles. The EDX pattern detailedly displays that the nanoparticles are composed of Mg, Sn, Ti, and O with an atomic ratio of Mg to Sn of ~3%. The characteristic current (I)−voltage (V) curves are displayed in Figure 6, and their

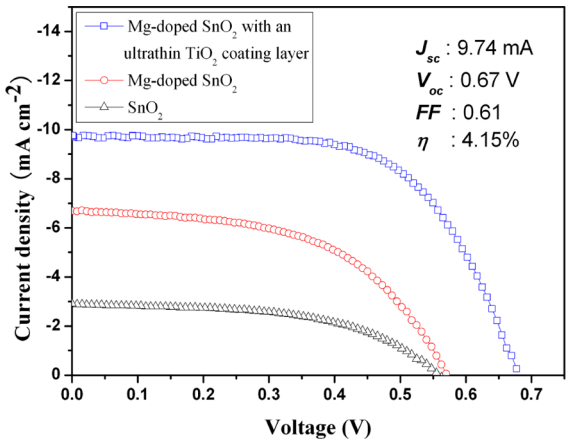

Figure 6. I−V curves of DSCs based on the pure SnO_2, Mg-doped SnO_2, and Mg-doped SnO_2 with an ultrathin TiO_2 coating layer photoelectrodes.

Table 1. Comparison of Photovoltaic Properties and Dye Loading of the DSCs

samples	J_{sc} (mA cm^{-2})	V_{oc} (mV)	FF (%)	η (%)	absorbed dye ($\times 10^{-8}$ mol cm^{-2})
SnO_2	2.87	0.56	52	0.85	7.13
Mg-doped SnO_2	6.69	0.57	53	2.03	7.87
Mg-doped SnO_2@ ultrathin TiO_2	9.74	0.67	61	4.15	9.42

[a]The active area of the photoelectrodes is 0.16 cm^2, [b]The dye adsorbed on SnO_2-based film was desorbed by a 0.1 M NaOH solution (water:ethanol 1:1 v/v) for 24 h.

photovoltaic parameters are summarized in Table 1. It can be seen that the short-circuit current (J_{sc}) for the Mg-SnO_2 electrode based DSC (6.69 mA cm^{-2}) is significantly higher than that of plain SnO_2 one (2.87 mA cm^{-2}); however, the Mg-SnO_2−TiO_2 device delivers the highest (9.74 mA cm^{-2}). In comparison to Mg-SnO_2, the further coated ultrathin TiO_2 layer in Mg-SnO_2−TiO greatly increases the dye adsorption as shown in Table 1, which could produces higher photocurrent. Interestingly, the open-circuit voltage (V_{oc} = 0.67 V) of the Mg−SnO_2−TiO_2 device also improved dramatically compared to both SnO_2 and Mg−SnO_2 devices, probably because of the passivation of the sub-band-edge surface states caused by magnesium doping into SnO_2 crystal framework and coating ultrathin TiO_2 layer.[22,23] Table 1 also shows that the Mg-SnO_2 device significantly boosts the overall power conversion efficiency (η) of the plain SnO_2 one from ~0.85% to ~2.03% and the Mg−SnO_2−TiO_2 device exhibits the remarkably highest η (4.15%), clearly demonstrating a synergic effect from the nanoengineered functionally multi-interfaced Mg−-SnO_2−TiO_2.

To further understand the synergic enhancement mechanism from the nanoengineered functionally multi-interfaced anode, we measured electrochemical impedance spectroscopy (EIS) of

dx.doi.org/10.1021/am3018493 | ACS Appl. Mater. Interfaces 2012, 4, 6261−6265

the DSCs. As shown in Figure 7, two well-defined semicircles in the Nyquist plots represent the charge transfer resistance of the

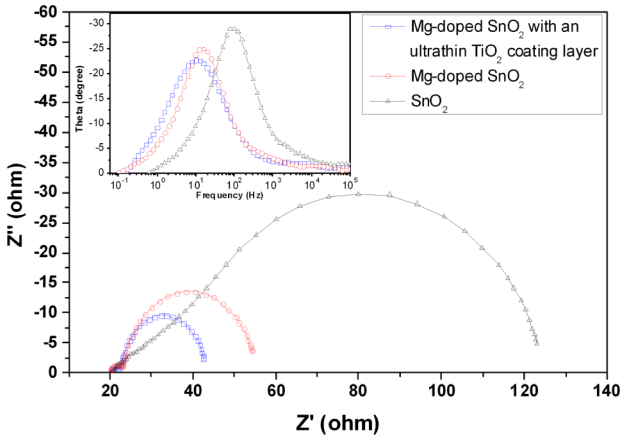

Figure 7. Nyquist and Bode diagrams (inset) of the EIS of DSCs based on the pure SnO_2, Mg-doped SnO_2 and Mg-doped SnO_2 with an ultrathin TiO_2 coating layer photoelectrodes.

redox reaction of I^-/I_3^- at the Pt/electrolyte interface (at high frequencies) and at the photoelectrode/electrolyte interface (in the region of low frequencies), respectively, of which a smaller diameter circle indicates slower charge transfer.[24−27] The semicircles for the Mg−SnO_2 photoanode has a much smaller diameter than that of the plain SnO_2 one, indicating much faster charge transfer ability; nevertheless, the Mg−SnO_2−TiO_2 anode even has the smaller diameter than that of the Mg-SnO_2 one by about two times, showing the highest charge transfer ability.

The frequency peak position (f_{max}) of the EIS semicircle in the Bode plots (Figure 7, inset) can be used to evaluate the charge recombination process at electrode/electrolyte/dye interfaces since electron lifetime $\tau_r = 1/2\pi f_{max}$ and a longer electron lifetime indicates less charge recombination.[28−32] The inset in Figure 7 illustrates that both SnO_2−Mg and SnO_2−Mg−TiO_2 photoanodes significantly shift f_{max} from 95 Hz for the plain SnO_2 to lower 10 and 9 Hz, respectively, which equals to 10 times longer electron lifetime than the plain SnO_2 electrode for a remarkably reduced charge recombination. However, *I*−*V* curve (see Figure S1 in the Supporting Information) shows that the photoanode made from coating an ultrathin TiO_2 layer on pure SnO_2 nanoparticles delivers a lower photocurrent density (5.93 mA cm^{-2}) and a close photovoltage (0.64 V) in comparison to the Mg-doped SnO_2. In contrast, the Mg-doped SnO_2 with an ultrathin TiO_2 coating layer exhibits much higher photocurrent density and photovoltage, clearly confirming that the great synergic effect of Mg doping in SnO_2 nanocrystals and further TiO_2 thin layer coating on significant performance improvement of solar cells. The mechanism for the Mg-doping to inhibit the charge recombination while enhancing the charge transfer is not clear and is still under investigation in our lab. However, we consider that this could be possibly explained by the "maze" structure of the doped magnesium within SnO_2 nanoparticles that can greatly prolong the light path for inhibiting the charge recombination process,[22] which also intimately corresponds to the IPCE spectra (seen in Figure 8). In contrast, the role of the TiO_2 layer in the further improvement of the device performance can be ascribed to its charge transfer enhancement, which is supported by the EIS results. This is understandable since the TiO_2 layer greatly increases the dye absorption (Table 1) over the SnO_2−Mg electrode, which can provide high electron injection rate to boost the charge transfer process.

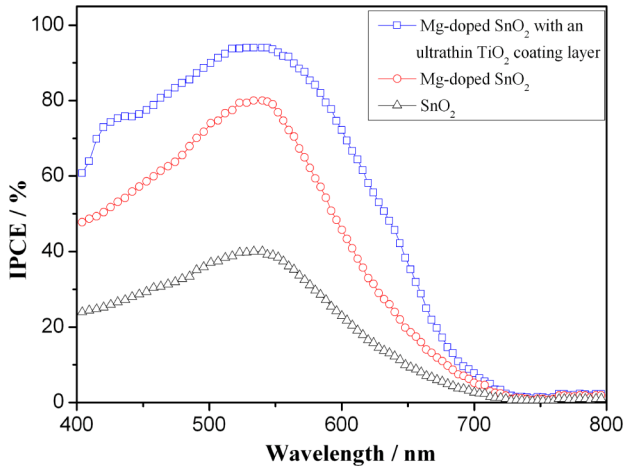

Figure 8. Normalized IPCE spectra of DSCs involving pure SnO_2, Mg-doped SnO_2 and Mg-doped SnO_2 with an untrathin TiO_2 coating layer.

4. CONCLUSION

In brief, a facile approach was used to construct functionally multi-interfaced SnO_2 photoanode with Mg-doping and TiO_2-coating for blocking charge recombination and enhancing charge transfer respectively in dye-sensitized solar cells. This synergic effect results in remarkably 5-fold improvement of power conversion efficiency (4.15%) over the plain SnO_2 based-device (0.85%). This work may imply that rationally engineering functionally multi-interfaced photoelectrode in nanoscales could be a universal approach to provide great potential for synergically boosting the performance of solar cells.

■ ASSOCIATED CONTENT

Supporting Information

This material is available free of charge via the Internet at http://pubs.acs.org.

■ AUTHOR INFORMATION

Corresponding Author

*E-mail: ecmli@swu.edu.cn.

Notes

The authors declare no competing financial interest.

■ ACKNOWLEDGMENTS

This work is financially supported by the Agency for Science, Technology and Research (A*STAR) under SERC Grant 102 170 0142.

■ REFERENCES

(1) Grätzel, M. *Nature* **2001**, *414*, 338.
(2) Qian, J.; Liu, P.; Xiao, Y.; Jiang, Y.; Cao, Y.; Ai, X.; Yang, H. *Adv. Mater.* **2009**, *21*, 3663.
(3) Atwater, H. A.; Polman, A. *Nat. Mater.* **2010**, *9*, 205213.
(4) Chen, T.; Guai, G. H.; Gong, C.; Hu, W.; Zhu, J.; Yang, H.; Yan, Q.; Li, C. M. *Energy Environ. Sci.* **2012**, *5*, 6294.

(5) Guai, G. H.; Leiw, M. Y.; Ng, C. M.; Li, C. M. *Adv. Mater.* **2012**, *2*, 334.
(6) Athews, D.; Wang, Q.; Pramana, S. S.; Lam, Y. M.; Mhaisalkar, S. *Nanoscale* **2011**, *3*, 4640.
(7) Guo, C. X.; Guai, G. H.; Li, C. M. *Adv. Mater.* **2011**, *1*, 448.
(8) Pang, H.; Yang, H.; Guo, C. X.; Lu, J.; Li, C. M. *Chem. Commun.* **2012**, *48*, 8832.
(9) Guo, C. X.; Yang, H. B.; Sheng, Z. M.; Lu, Z. S.; Song, Q. L.; Li, C. M. *Angew. Chem., Int. Ed.* **2010**, *49*, 3014.
(10) Sun, P.; Zhang, X.; Liu, X.; Wang, L.; Wang, C.; Yang, J.; Liu, Y. *J. Mater. Chem.* **2012**, *22*, 6389.
(11) Birkel, A.; Lee, Y.; Koll, D.; Meerbeek, X. V.; Frank, S.; Choi, M. J.; Kang, Y. S.; Char, K.; Tremel, W. *Energy Environ. Sci.* **2012**, *5*, 5392.
(12) Wang, Z.; Zhou, L.; Lou, X. W. *Adv. Mater.* **2012**, *24*, 1903.
(13) Du, J.; Qi, J.; Wang, D.; Tang, Z. *Energy Environ. Sci.* **2012**, *5*, 6914.
(14) (a) Djojoputro, H.; Zhou, X. F.; Qiao, S. Z.; Wang, L. Z.; Yu, C. Z.; Lu, G. Q. *J. Am. Chem. Soc.* **2006**, *128*, 6320. (b) Snaith, H.; Ducati, C. *Nano Lett.* **2010**, *10*, 1259.
(15) (a) Krishnamoorthy, T.; Tang, M. Z.; Verma, A.; Nair, A. S.; Pliszka, D.; Mhaisalkar, S. G.; Ramakrishna, S. *J. Mater. Chem.* **2012**, *22*, 2166. (b) Wang, W.; Li, J.; Hou, Y.; Yu, Y.; Su, C.; Kuang, D. *Chem.—Eur. J.* **2010**, *16*, 8620.
(16) Ramasamy, E.; Lee, J. *Energy Environ. Sci.* **2011**, *4*, 2529.
(17) Kay, A.; Gratzel, M. *Chem. Mater.* **2002**, *14*, 2930.
(18) Pang, H.; Ning, G.; Gong, W.; Ye, J.; Lin, Y. *RSC Advances* **2011**, *1*, 184.
(19) Wagner, C. D.; Biloen, P. *Surf. Sci.* **1973**, *35*, 82.
(20) Thomas, T. D.; Weightman, P. *Phys. Rev. B.* **1986**, *33*, 5406.
(21) Seyama, H.; Soma, M. *J. Chem. Soc., Faraday Trans.* **1984**, *80*, 237.
(22) Feng, X.; Shankar, K.; Paulose, M.; Grimes, C. A. *Angew. Chem., Int. Ed.* **2009**, *48*, 8095.
(23) Peng, Z. A.; Peng, X. G. *J. Am. Chem. Soc.* **2001**, *123*, 1389.
(24) Li, C. M.; Chen, W.; Yang, X. *Front Biosci.* **2005**, *10*, 2518.
(25) Li, C. M.; Sun, C. Q.; Song, S.; Choong, V. E.; Maracas, G.; Zhang, X. J. *Front Biosci.* **2005**, *10*, 180.
(26) Yang, H.; Song, Q.; Lu, Z.; Guo, C.; Gong, C.; Hu, W. H.; Li, C. M. *Energy Environ. Sci.* **2010**, *3*, 1580.
(27) Chen, G. H.; Gong, C.; Hu, W. H.; Zhu, J. X.; Yang, H. B.; Yan, Q. Y.; Li, C. M. *Energy Environ. Sci.* **2012**, *5*, 6294.
(28) Lu, Z. S.; Guo, C. X.; Yang, H. B.; Qiao, Y.; Guo, J.; Li, C. M. *J. Colloid Interface Sci.* **2011**, *353*, 588.
(29) Yang, H. B.; Guo, C. X.; Guai, G. H.; Song, Q. L.; Jiang, S. P.; Li, C. M. *ACS Appl. Mater. Interfaces* **2011**, *3*, 1940.
(30) Fabregat-Santiago, F.; Bisquert, J.; Palamares, E.; Otero, L.; Kuang, D. B.; Zakeeruddin, S. M.; Gratzel, M. *J. Phys. Chem. C* **2007**, *111*, 6550.
(31) Yang, H.; Guai, G. H.; Guo, C. X.; Song, Q. L.; Jiang, S. P.; Wang, Y. L.; Zhang, W.; Li, C. M. *J. Phys. Chem. C* **2011**, *115*, 12209.
(32) Wang, Q.; Moer, J. E.; Gratzel, M. *J. Phys. Chem. B* **2005**, *109*, 14945.